Temperature and density dependence of Kr L-shell spectrum in hot dense plasmas

6 authors, including:

Enac gallardo-diaz
University of Nevada, Reno
5 PUBLICATIONS **1** CITATION

SEE PROFILE

Ricardo Florido
Universidad de Las Palmas de Gran Canaria
102 PUBLICATIONS **932** CITATIONS

SEE PROFILE

Temperature and density dependence of Kr L-shell spectrum in hot dense plasmas

E. Gallardo-Diaz ✉ ⓘ ; R. C. Mancini ⓘ ; K. R. Carpenter ⓘ ; P. Adrian ⓘ ; J. Frenje ⓘ ; R. Florido ⓘ

Check for updates

View Online   Export Citation   CrossMark

Temperature and density dependence of Kr L-shell spectrum in hot dense plasmas

View Online   Export Citation   CrossMark

E. Gallardo-Diaz,[1,a)] (iD) R. C. Mancini,[1] (iD) K. R. Carpenter,[1,b)] (iD) P. Adrian,[2] (iD) J. Frenje,[2] (iD) and R. Florido[3] (iD)

AFFILIATIONS

[1]Physics Department, University of Nevada, Reno, Nevada 89557, USA
[2]Plasma Science Fusion Center, Massachusetts Institute of Technology, Massachusetts 02139, USA
[3]iUNAT-Departamento de Física, Universidad de Las Palmas de Gran Canaria, 35017 Las Palmas de Gran Canaria, Spain

[a)]Author to whom correspondence should be addressed: enacgallardo@nevada.unr.edu
[b)]Currently at Lawrence Livermore National Laboratories.

ABSTRACT

Kr L-shell spectroscopy modeling results are discussed in this paper, focusing on the n = 4 to n = 2 line transitions of Be- and Li-like Kr ions. Collisional radiative atomic kinetic and Stark-broadened spectral line shape calculations show electron temperature T_e and density n_e sensitivity in the spectrum. The combination of the T_e dependence due to the relative intensity of Be-like to Li-like line emissions in the range from 1.5 to 3 keV and the n_e sensitivity from the Stark broadening effect on the line shapes in the range from 5×10^{23} to 2×10^{24}/ cc results in a spectrum that can be employed to diagnose T_e and n_e. Two different collisional radiative atomic kinetic models i.e., Prismspect [J. J. MacFarlane, *et al.*, Int. Fusion Sci. Appl. Conf. Proc. **457** (2003)] and ABAKO [Florido, *et al.*, PRE, **80**, 056402 (2009)] produce similar results in level populations and spectra. In x-ray spectroscopy of implosion cores, this Kr L-shell spectrum may prove useful in an intermediate T_e range in which Ar is too ionized for its K-shell to be of diagnostic value and Kr is not ionized enough for its K-shell emission to be useful.

I. INTRODUCTION

Hot dense plasma is a state of matter which is present under extreme conditions of temperature and density. Because of these extreme conditions, the measurement or diagnostic of the plasma's temperature and density presents a significant challenge. One approach to conduct this diagnosis is through x-ray spectroscopy of suitable elements and transitions. The interpretation and analysis of the plasma radiation self-emission (or that of a tracer) and/or absorption can provide accurate measurements of temperature and density. These measurements are key to understand different physical processes in the plasma which depend on these conditions. For example, in high-energy density plasma experiments, x-ray spectroscopy has been used to validate low-Z stopping power formalisms.[1,2] Moreover, in the dense core plasmas of inertial confinement fusion (ICF) experiments, tracer x-ray spectroscopy has been crucial to diagnose space and/or time-resolved temperature and density at the stagnation of the implosion.[3–13] ICF has been an important nuclear fusion energy approach in the last few decades. In these experiments, a millimeter scale capsule containing the fusion fuel (deuterium and tritium) is driven directly or indirectly by high-power laser beams. The intense radiation ablates the outer part of the shell making the inner part

implode the fuel in the core, thus rising the temperature and density of the fuel and reaching nuclear fusion conditions. X-ray spectroscopy has been used in ICF experiments for several years at facilities like OMEGA[3–9] and the National Ignition Facility (NIF).[11–14] More recently, this technique has also been used in the alternative ICF approach MagLIF at the Z-machine.[15–17] X ray emission spectroscopy diagnostics use the radiation emitted from tracer quantities of a higher Z element in the capsule to infer the electron temperature (T_e) and density (n_e). These are key magnitudes to characterize the state of the burning plasma. When the conditions of the plasma are such that the self-emission is not useful for diagnostics, x-ray absorption spectroscopy can still be used to extend the usefulness of the spectroscopic method.[18–20]

Argon K-shell emission has been used extensively as the spectroscopic signature of implosion experiments for around two decades.[3–5,7–9,16,17] However, in hot implosion cores ($T_e > 2$ keV), argon becomes less useful as a spectroscopic tracer as it becomes too ionized. Krypton has been studied recently as an alternative to argon to overcome this problem.[11–15] Kr L-shell emission may be used as a plasma diagnostic for hot implosions ($T_e = 1.5 - 3$ keV), while Kr K-shell emission may be used for this purpose in even hotter implosions. For this reason, Kr L-shell emission can bridge the range of T_e between Ar

and Kr K-shell. While K-shell spectroscopy provides a more simple spectrum due to the reduced number of line transitions, L-shell spectroscopy has also been used to diagnose plasma conditions in the past.[21–25] In this paper, we use different models to simulate the atomic kinetics and Stark line broadening of a typical implosion core plasma containing krypton to study the sensitivity of the L-shell emission to changes in electron temperature and density.

The development of the Kr L-shell spectroscopic diagnostic technique shown here is general. However, in this research, it is applied to the study of nuclear fusion product's stopping power and ion-electron thermal equilibration in OMEGA implosions.[1,2] These phenomena are dependent on local conditions of T_e and n_e. The objective of this paper is to develop the theoretical modeling necessary to then obtain plasma condition measurements which help to understand these plasma processes. The choice of plasma components, concentrations, and conditions in the model are the ones expected in these type of experiments.

This paper is organized as follows: Sec. II describes the study of the electron temperature sensitivity using collisional radiative atomic kinetics to simulate plasma conditions and find line ratios which are electron temperature dependent. Section III describes the study of the electron density sensitivity using detailed Stark broadening calculations and discusses the dependence of the spectral line shape with the electron density. Section IV shows the results of combining the information provided by the collisional-radiative model and detailed Stark broadening calculations to create synthetic spectra for the case of a uniform spherical plasma source. Conclusions are discussed in Sec. V.

II. COLLISIONAL-RADIATIVE MODELS AND ELECTRON TEMPERATURE SENSITIVITY

In this section, we describe the plasma model that we use in our simulations and compare the results of two collisional radiative atomic kinetic models, namely, Prismspect[26] and ABAKO[27] in order to assess the impact of different sources of atomic physics modeling. Each model uses a different atomic database: ATBASE in the case of Prismspect and Flexible Atomic Code (FAC[28]) in the case of ABAKO. The main difference between the two collisional radiative models consists in the calculation of the atomic kinetics rates which in the case of Prismspect uses a full quantum-mechanical calculation, while ABAKO uses analytic approximations.

The model of our plasma is an implosion spherical core with a 50 μm radius containing 50% (atomic concentration) D, 50% ^{3}He, and a small concentration of Kr. The krypton atomic model used is described in detail in Table II of Ref. 27. The two models solve the atomic kinetics rate equations in the plasma self-consistently with the radiation transport equation. The solutions of the model provide the atomic level population and the emergent intensity distribution from the plasma using Voigt spectral line shapes. The following atomic processes are included in the model: electron collisional excitation and de-excitation, electron collisional ionization and recombination, photo excitation and stimulated emission, photo ionization and stimulated recombination, auto-ionization and electron capture, radiative recombination and spontaneous emission. Only electric dipole allowed transitions (E1) were included in the models. In both cases, the calculations of the atomic level populations were performed in the Detailed Configuration Accounting (DCA) approximation.[29] We have tested the validity for our density conditions of this approximation by comparing with simulations which did not include this approximation, confirming that the difference in the results was negligible. This shows

that for our plasma conditions, the populations of fine structure energy levels within the configurations are in equilibrium. Finally, we assume that the free electrons in the plasma are in thermal equilibrium and described by a Maxwellian distribution characterized by an electron temperature T_e. We consider the steady-state approximation usually employed in dense implosion core plasmas in which timescales for the change of the plasma conditions are significantly longer than the timescales of the atomic processes determining the level population kinetics.[8] We study the parameter space formed by $T_e = 1 - 4$ keV and $n_e = 5 - 50 \times 10^{23}$/cc relevant to our case of application.

In this section, we first show the kinetic results (Sec. II A) and the dependence of the ion and level population with the plasma conditions and, second, the spectral results (Sec. II B) and the spectral dependence with the conditions and tracer concentration. The figures in this section show results from Prismspect unless stated otherwise.

A. Plasma kinetic results

A study of the charge state distribution dependence with the expected range of conditions of our plasma is performed. Figure 1 shows the fractional population T_e dependence of the different krypton ions for a Prismspect simulation of a plasma containing 0.04% of krypton concentration and at an electron density of 10^{24}/cc. We observe how the increase in temperature shifts the charge state distribution toward more ionized states as expected. Within the L-shell charge states (Li- to Ne-like), Li- and Be-like are the most dominant ones. The change in the fractional population of these ions with respect to electron temperature is shown in Fig. 2. In this figure, we observe the difference on the electron temperature dependence of the fractional population of both ions for ABAKO and Prismspect simulations. The two collisional radiative models show a similar dependence of the fractional population with electron temperature. However, there is a larger difference in the case of the Li-like fractional population. The increase in temperature between 1.5 and 4 keV decreases the fractional population of Be-like ions which means that the charge state distribution is shifting to higher charge states. This is consistent with the Li-like curve which starts increasing from 1.5 to 2 keV and peaks between 2 and 2.5 keV. In this region of temperatures, the Be-like ions are becoming ionized, thus feeding the Li-like charge state. In the range of 2.5 to 4 keV, the Li-like fractional population decreases with increasing T_e.
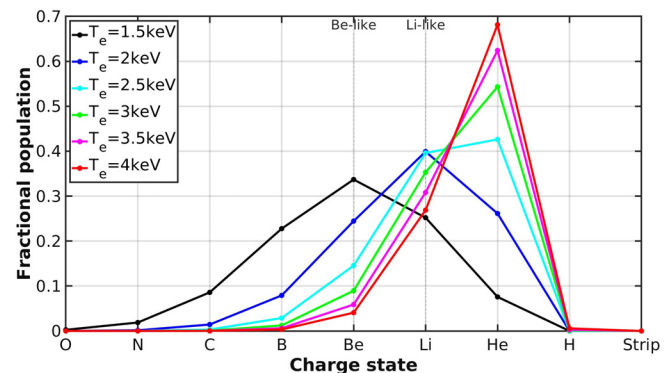

FIG. 1. Kr charge state distribution for different electron temperatures calculated with Prismspect at $n_e = 10^{24}$/cc.
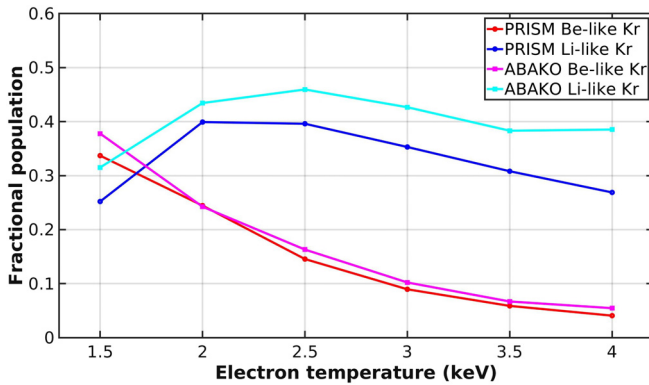
FIG. 2. Li- and Be-like fractional population dependence with electron temperature calculated with Prismspect and ABAKO at $n_e = 10^{24}$/cc.

This shows the ionization of Li-like into He-like Kr. The ratio of the Be-like over Li-like populations for each code is shown in Fig. 3. From this figure, we observe the electron temperature sensitivity of the relative populations between these two ions. The sensitivity decreases with electron temperature.

The intensity of a line transition is proportional to the population of the upper level of said transition. As we will discuss in Sec. II B, our spectral range of interest includes Be- and Li-like transitions from n = 4 to n = 2. Namely, $1s^2 2l4l' \rightarrow 1s^2 2l2l'$ and $1s^2 4l \rightarrow 1s^2 2l$, respectively. Here, l and l' represent the orbital's angular momentum ranging from 0 to $n - 1$, where n is the principal quantum number. As the models only calculate E1 transitions, the upper levels of these transitions are $1s^2 2l4l^*$ and $1s^2 4l^*$, respectively, where l^* includes the s, p, and d subshells but not the f one following the selection rules. The ratio between the population of these levels is displayed in Fig. 4. This plot shows the T_e sensitivity of the relative population of the upper levels corresponding to the Be- and Li-like transitions of interest, suggesting that the relative emission between these Be- and Li-like transitions can be used as an electron temperature diagnostic. We emphasize though, that f subshells have been included in the atomic kinetic calculations.

The charge state distribution of the krypton in the plasma also depends on the electron density. Figure 5 shows the n_e dependence of
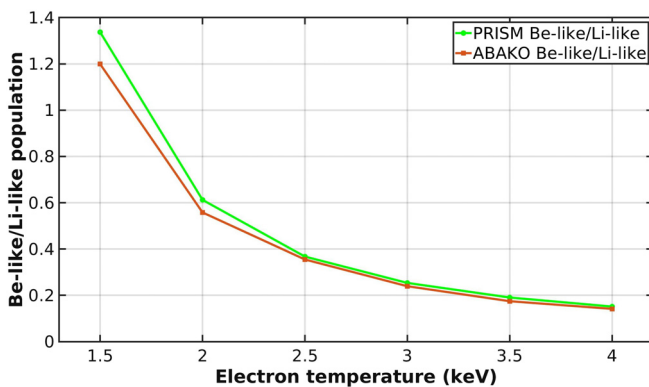

FIG. 3. Ratio of the Be- and Li-like ion population with respect to electron temperature calculated with Prismspect and ABAKO at $n_e = 10^{24}$/cc.
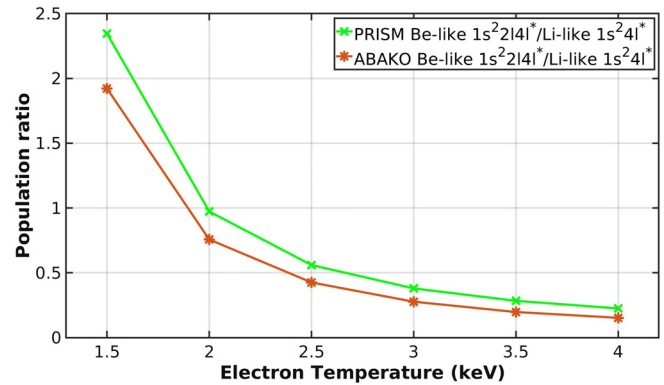

FIG. 4. Ratio of the Be-like $1s^2 2l4l^*$ and Li-like $1s^2 4l^*$ level population with respect to electron temperature calculated with Prismspect and ABAKO at $n_e = 10^{24}$/cc. l^* includes the s, p, and d sub-shells but not the f one.
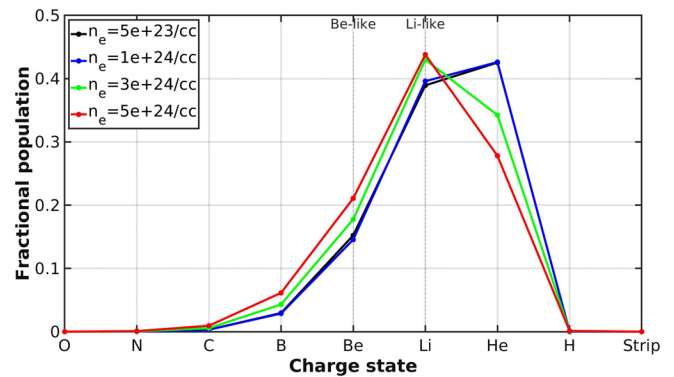

FIG. 5. Kr charge state distribution for different electron densities calculated with Prismspect at $T_e = 2.5$ keV.

the charge state distribution for an electron temperature of 2.5 keV. The different distributions span over an order of magnitude range in n_e, but the change is not so notable as the change with T_e in Fig. 1. From the comparison of these two figures, it is also clear that the change in relative population of Be- and Li-like ions with n_e is small compared to the one with T_e. For these dense plasma conditions, the increase in electron density in the plasma increases the recombination rate over the ionization one and we can note how the charge state distribution shifts toward lower charge states.

B. Line spectra results

The spectral region of interest of the Kr L-shell emission is shown in Fig. 6. This figure shows the spectrum of the n = 4 to n = 2 transitions as well as the contribution breakdown from the different ions. The plasma conditions in this simulation are $T_e = 2$ keV, $n_e = 10^{24}$/cc. The two main ion contributions to the spectrum are from Li- and Be-like Kr. The Kr Li-like transitions are labeled with letters from A to D and detailed in Table I. The n = 4 to n = 2 transitions were chosen as diagnostic lines because of two reasons: they are relatively well isolated presenting little overlap between different ion
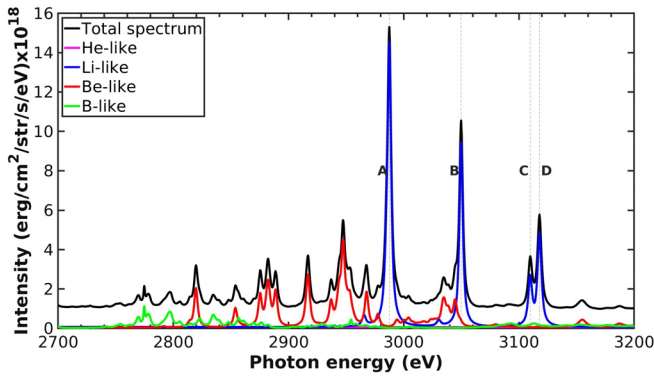
FIG. 6. Kr L-shell total emission and ion contribution breakdown in the spectral region of interest. The electronic transitions in this region are from n = 4 to n = 2. 0.04% Kr concentration in the plasma. $T_e = 2$ keV, $n_e = 10^{24}$ / cc. Uniform sphere, radius = 50 μm. The main Kr Li-like transitions are labeled from A to D and are specified in Table I.

TABLE I. Main Li-like Kr (E1) transitions from n = 4 to n = 2. From ATBASE.

Line ID	Photon energy (eV)	Upper level	Lower level
A	2984.88	$1s^2 4d \ ^2D_{3/2}$	$1s^2 2p \ ^2P_{3/2}$
	2987.49	$1s^2 4d \ ^2D_{5/2}$	$1s^2 2p \ ^2P_{3/2}$
B	3049.81	$1s^2 4d \ ^2D_{3/2}$	$1s^2 2p \ ^2P_{1/2}$
C	3109.77	$1s^2 4p \ ^2P_{1/2}$	$1s^2 2s \ ^2S_{1/2}$
D	3117.83	$1s^2 4p \ ^2P_{3/2}$	$1s^2 2s \ ^2S_{1/2}$

contributions and the spectral range is close to the one used for the Ar K-shell diagnostic instruments in the past like the multi-monochromatic x-ray imager.[30]

The krypton L-shell spectra for different electron temperatures are shown in Fig. 7. This figure shows the spectra obtained from the same Prismspect simulation with 0.04% Kr concentration in the plasma and an electron density of 3×10^{24}/cc. Each line represents
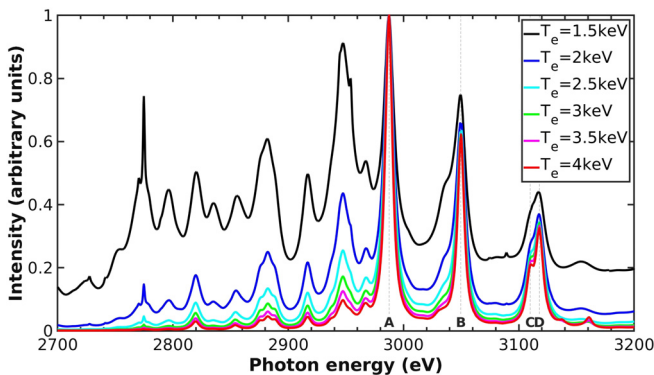

FIG. 7. Kr L-shell bound-bound emission for different plasma electron temperatures. Each spectra is normalized to the main Li-like transition A. $n_e = 3 \times 10^{24}$ / cc. Uniform sphere, radius = 50 μm. The main Kr Li-like transitions are labeled from A to D and are specified in Table I.

the spectra for a given temperature, and they are all normalized to Li-like transition A. We observe a change in the relative emission between the Li-like main line transitions (A–D) and the Be-like emission at lower photon energy. As we expected from the upper level population ratio in Fig. 4, we observe a decrease in the Be-like emission compared to the Li-like one as the electron temperature increases. This plot also shows the decrease in the sensitivity at higher electron temperatures. At approximately $T_e = 3$ keV, both the sensitivity and the level of Be-like emission become low which compromises its application as an electron temperature diagnostic. However, this spectral region may be used as electron temperature diagnostic for electron temperatures between 1.5 and 3 keV.

From the simulations of the collisional radiative codes, we can also estimate which Kr tracer concentrations in the plasma would be suitable for L-shell emission diagnostic purpose. A suitable concentration is a trade-off between three conditions: (1) high enough to produce a quality signal that allows detailed analysis but (2) small enough to keep radiation transport effects low and (3) also small enough to minimize the possible impact on implosion hydrodynamics.

We study the first two conditions by comparing the Kr simulated spectra to Ar signal levels in typical conditions which have been experimentally studied before (0.18% Ar, $T_e = 1.5$ keV, $n_e = 10^{24}$ / cc).[31] Figure 8 shows the intensity comparison between Kr and Ar, while Fig. 9 compares their optical depths. In these figures, the main Kr Li-like transitions are labeled with letters from A to D and the main Ar K-shell lines used for diagnostics (He-β, Ly-β, and Ly-γ)[5–7] are also labeled. The Ar He-α and Ly-α are not shown as they are optically thick and, thus, less reliable for diagnostic purpose. However, it is worth noting that they overlap with the Kr n = 4 to n = 2 transitions which would difficult the simultaneous use of Ar and Kr spectroscopic tracers for a given experiment. From these two figures, we can observe that for a Kr concentration in the plasma between 0.02% and 0.04% the intensity of the main Kr lines is comparable or larger than the one of the Ar lines while the optical depth is lower (and less than one). An optical depth lower than one means that the mean free path of the photon is larger than the length scale of the plasma which translates in
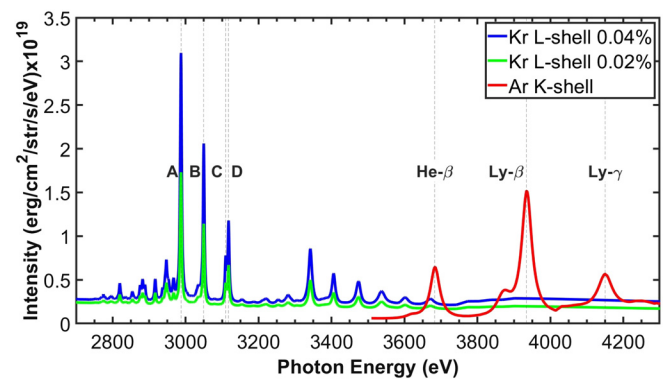

FIG. 8. Signal comparison between Ar K-shell and Kr L-shell simulated spectra for different concentrations in the plasma. Ar simulation conditions are typical ICF experiment conditions:[31] 0.18% concentration, $T_e = 1.5$ keV and $n_e = 10^{24}$ / cc. Kr simulation conditions: $T_e = 2.5$ keV and $n_e = 10^{24}$ / cc. For both simulations, we model a uniform spherical plasma of radius = 50 μm. The main Kr Li-like transitions are labeled from A to D and are specified in Table I. The main Ar K-shell transitions which are usually used for plasma diagnostics are also labeled.
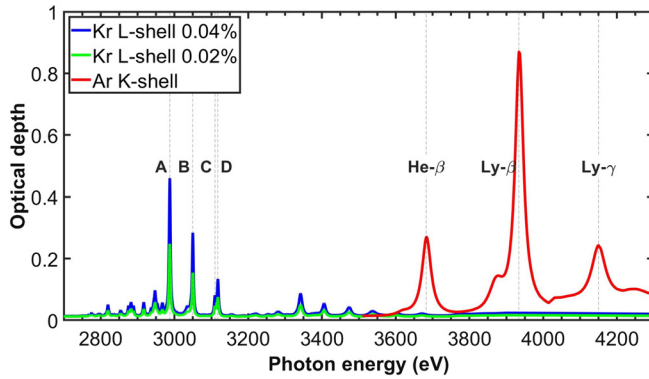
FIG. 9. Optical depth comparison between Ar K-shell and Kr L-shell simulated spectra for different concentrations in the plasma. Simulation conditions are the ones specified in Fig. 8.

low opacity effects. Consequently, these two concentrations of Kr in the plasma (0.02% and 0.04%) satisfy the first two conditions.

Since the Kr lines are narrower and closer together compared to the Ar lines, we examined the impact of the instrumental response in the spectra. To this end, the spectra illustrated in Fig. 8 was convolved with a Gaussian function of 20 eV, simulating the response of a spectrometer with a modest resolving power of approximately 150. The results reveal a reduction of the Kr peak signal relative to the Ar one due to the narrower line shape. However, the signal levels remain comparable between the two spectral regions for these Kr concentrations. Moreover, the relevant Kr Li- and Be-like lines remain resolved even after applying the finite spectral resolution, enabling the data analysis.

The third condition needs to be studied with a hydrodynamic model and the effects may be experiment dependent. The range of concentrations between 0.02% and 0.04% is comparable to the Kr concentrations used at the NIF and discussed in Chen's paper.[12] Without loss of generality, we use these concentrations in this research.

III. DETAILED STARK BROADENING LINE SHAPES AND ELECTRON DENSITY SENSITIVITY

The detailed Stark broadening spectral line shape calculations were performed using the multi-electron Stark-broadened line shape model and code (MERL)[32] using Cowans atomic database.[33] The results of the simulations in this section correspond to plasma conditions of $T_e = 2$ keV and $n_e = 10^{24}$/ cc unless stated otherwise. The Stark broadening is produced by the electric micro-fields due to the electrons and ions in the plasma. In our case, this effect is modeled following the standard Stark broadening theory approximation,[34] i.e., dynamic electrons and static ions. Accordingly, the line shape $\phi(h\nu)$ is given by the following expression:

$$\phi(h\nu) = \int P(\varepsilon)J(h\nu, \varepsilon)d\varepsilon, \quad (1)$$

where $\varepsilon = \frac{E}{E_o}$ is the electric micro-field normalized to a reference micro-field (E_o) given in terms of the electron's charge and sphere radius $[r_o = (\frac{3}{4\pi n_e})^{1/3}]$. In Eq. (1), $P(\varepsilon)$ corresponds to the static ion micro-field distribution function and $J(h\nu, \varepsilon)$ to the electron broadening function. This function contains the effects on line transitions of the impact broadening of the electrons and the split and shift of energy

levels due to the ion's static Stark effect for a single microfield value ε. The interaction between the atomic radiator and the perturbing plasma electrons and ions is taken into account in a dipole approximation.

The Stark effect mixes field-free atomic states with same magnetic quantum number M and different angular momentum quantum number J. For this reason, M is still a good quantum number while J is not. For a given J, the energy levels corresponding to different M states are degenerate when the electric micro-field is zero. However, when the micro-field is increased, this degeneracy is removed. As we increase ε, the separation between the energy levels increases due to the linear dependence of the perturbation with the field. This effect shifts the energy levels of the upper and lower states of all transitions. As we will show below, this causes the line profile of the transitions to change significantly producing double peak structures and more complex shapes.

The J function also contains the information of the dynamic electron broadening. This effect is produced by the collisions between the free electrons in the plasma and the radiator. In our model, we consider the duration of these collisions to be much shorter than the excited state's lifetime i.e., the impact approximation. This effect results in a Lorentzian line profile with a characteristic width that depends on the electron density n_e. Natural and thermal Doppler broadening are also taken into account in the J function.

The $J(h\nu, \varepsilon)$ is plotted in Fig. 10 for different values of ε. The labeled transitions corresponding to the ones listed in Table I are only valid for $\varepsilon = 0$ as the states become mixed at non-zero fields. For this case, the line shapes compare well to the ones obtained from the Prismspect simulations in the previous section (Fig. 6). This is because Prismspect includes only the electron broadening effect but does not calculate the energy level shift due to the static ion's Stark effect. For the case $\varepsilon = 1$, the J function shows the transitions between the shifted upper and lower energy levels. In the case of the A and B transitions, the single peak structure is transformed into a double peak structure. When we increase the field to $\varepsilon = 2$, the separation between the peaks of these transitions increases and new spectral structure develops. This is the result of a stronger mix of states and, thus, a larger energy shift and more field-dependent transitions. This effect is similar to that noted in the double-peak structure of the β-lines in the He- and H-like
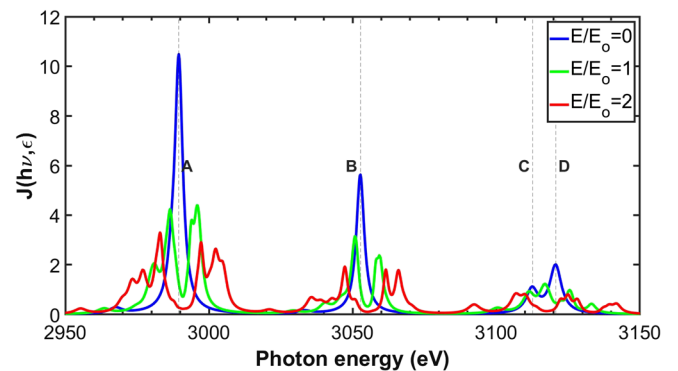

FIG. 10. Electron broadening function $J(h\nu, \varepsilon)$ calculated with MERL for the Li-like Kr n = 4 to n = 2 transitions for different values of ε at $T_e = 2$ keV and $n_e = 10^{24}$/ cc. The main Kr Li-like transitions are labeled from A to D and are specified in Table I which correspond to the zero field case.

FIG. 11. Line profile for Li-like Kr n = 4 to n = 2 transitions at $T_e = 2$ keV and $n_e = 10^{24}/$ cc. The main Kr Li-like transitions are labeled from A to D and are specified in Table I which correspond to the zero field case.
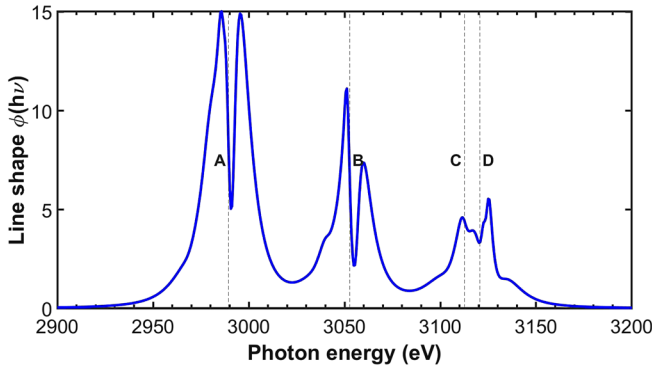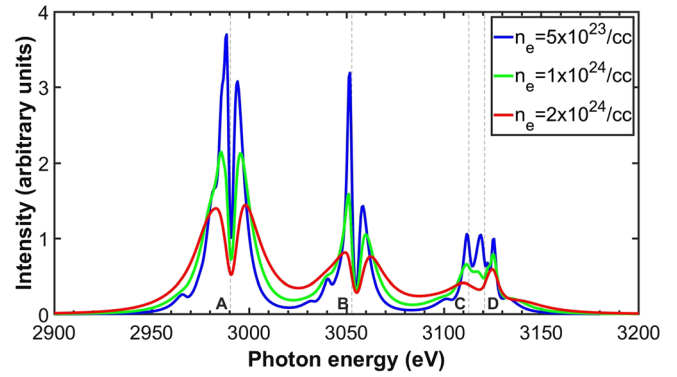

FIG. 12. MERL calculation results for Stark broadened line-shapes of Kr Li-like transitions from $1s^2 4l$ to $1s^2 2l$ for $T_e = 2$ keV. The main Kr Li-like transitions are labeled from A to D and are specified in Table I which correspond to the zero field case.
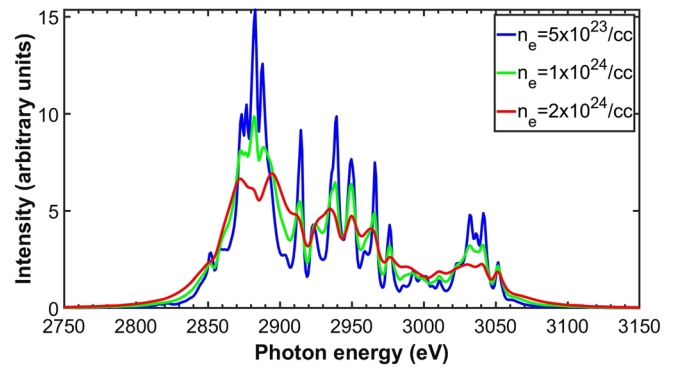

FIG. 13. MERL calculation results for Stark broadened line-shapes of Kr Be-like transitions from $1s^2 2l4l'$ to $1s^2 2l2l'$ for $T_e = 2$ keV.

ions of K-shell spectrum. However, in this L-shell spectrum, it is present in n = 4 to n = 2 transitions.

At this point, we have shown what the *J* function looks like for a given value of ε. However, in the plasma, there is not a single value of the micro-field but a distribution of values characterized by the static ion micro-field distribution $P(\varepsilon)$. In this work, we have employed the APEX model to compute this distribution[35,36] and perform the integral over microfield values that produce the spectral line shape.

Figure 11 shows the spectral line shape for the case of the Li-like Kr transitions from n = 4 to n = 2. The labels from A to D correspond to the energy of the transitions in the zero field case specified in Table I. We observe that after the integration we obtain the double peak structure similar to the one of the *J* function for the case $\varepsilon = 1$ in Fig. 10. This is because the peak of the micro-field distribution function is close to $\varepsilon = 1$. However, the wings have become broader filling the valleys between peaks. We note that for multi-element plasmas where the majority of perturbing ions are light ions like deuterium, the ion dynamics effect should make a noticeable contribution to the Stark-broadened line shapes. As it was shown in Ref. 38 for the case of the Ar K-shell spectrum, this effect will round sharp peaks, partially fill the valley between double-peak structures, and increase overall line broadening by a small amount. This effect should be included before applying model calculations to data analysis to extract the most accurate plasma temperature and density values. However, the focus of this work has been to emphasize the dramatic effect produced by the field mixing driven by static ions that results in characteristic line splitting, double peak structures, and broadening of the spectrum.

We have calculated the line profiles for different electron densities to study their dependence. The dependence of Li- and Be-like Kr transitions from n = 4 to n = 2 is shown in Figs. 12 and 13, respectively. We have followed the same procedure to obtain the Be-like line profiles of the transitions from $1s^2 2l4l'$ to $1s^2 2l2l'$. These show a more complex and richer line spectrum than the Li-like ones due to the higher complexity of the atomic structure. As shown in the Figs. 12 and 13, the increase in the electron density increases the magnitude of the electric micro-field which translates in a stronger Stark effect and thus a larger state mixing and energy level shift as well as the electron broadening effect. Both figures show not only the linewidth increase with n_e but the line profiles significant change. There is a good n_e

sensitivity from 5×10^{23} to $2 \times 10^{24}/$ cc. Thus, the plasma electron density can be inferred using the line profile n_e sensitivity in this range.

For completeness, Fig. 14 shows the area normalized Li-like line profiles for different electron temperatures at $n_e = 10^{24}/$cc. This figure shows there are some features of the profile that have some T_e dependence. However, this effect is small compared to the dependence with the electron density shown in Fig. 12.

IV. THE EMERGENT INTENSITY DISTRIBUTION

In previous sections, we have shown the electron temperature and density sensitivity of the Kr L-shell spectra. In this section, we will show how we combine both effects and calculate the radiation transport through the plasma to obtain the emergent intensity distribution. We first calculate the emissivity $(j(h\nu))$ and opacity $(k(h\nu))$ which are intrinsic properties of the plasma

$$j(h\nu) = \sum_{\alpha\beta} \frac{h\nu}{4\pi} N_\beta A_{\beta\alpha} \Phi_{\alpha\beta}(h\nu), \qquad (2)$$

$$k(h\nu) = \sum_{\alpha\beta} \frac{h\nu}{4\pi} (N_\alpha B_{\alpha\beta} - N_\beta B_{\beta\alpha}) \Phi_{\alpha\beta}(h\nu), \qquad (3)$$
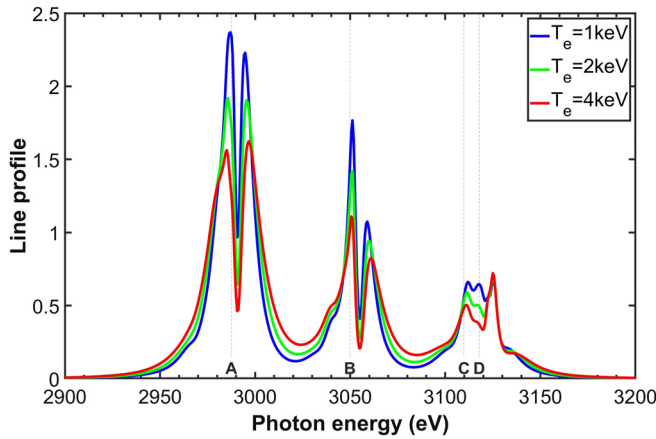
FIG. 14. MERL calculation results for Stark broadened line-shapes of Kr Li-like transitions from $1s^2 4l$ to $1s^2 2l$ for $n_e = 10^{24}$/cc. The main Kr Li-like transitions are labeled from A to D and are specified in Table I which correspond to the zero field case.

where α and β represent the lower and upper states of each transition, respectively. N_α is the population of α level, $\Phi_{\alpha\beta}(h\nu)$ is the line profile, and $A_{\alpha\beta}$ and $B_{\alpha\beta}$ are the Einstein coefficients of the transition from state α to state β. From the collisional-radiative atomic kinetic calculations, we obtain the level population N_α and the atomic rates for each plasma condition pair of T_e and n_e. The detailed Stark broadening calculations provide the line profile $\Phi_{\alpha\beta}(h\nu)$ for each transition. Performing the summatories shown in Eqs. (2) and (3), we obtain $j(h\nu)$ and $k(h\nu)$. This method assumes that the upper levels of each line shape are in LTE within themselves i.e., LTE within $1s^2 4l$ and within $1s^2 2l4l'$. This assumption is valid for the conditions studied in this paper.

We use the radiation transport solution for the case of a uniform sphere discussed in reference[38] to model the effect of the finite size plasma into the spectra. The result of this calculation is the emergent intensity distribution $I(h\nu)$. Figure 15 shows the emergent intensity
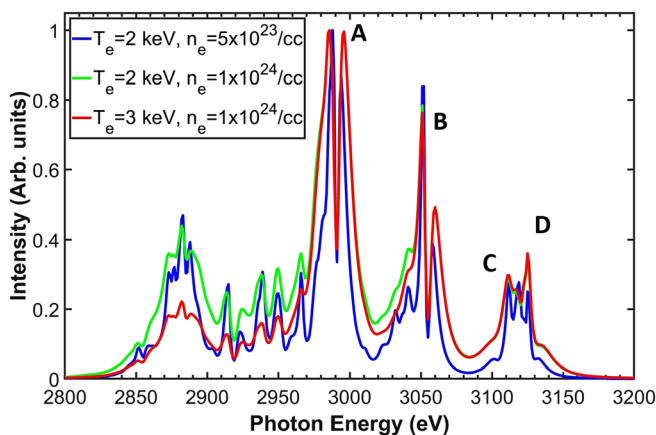

FIG. 15. Emergent intensity distribution of Be- and Li-like Kr n = 4 to n = 2 transitions for different conditions of a uniform spherical plasma with $r = 50\,\mu$m. The main Kr Li-like transitions are labeled from A to D and are specified in Table I. The spectra are normalized to the most intense peak of line A.

FIG. 16. Emergent intensity distribution of Be- and Li-like Kr n = 4 to n = 2 transitions for $T_e = 2$ keV and $n_e = 10^{24}$/cc using a uniform spherical plasma with $r = 50\,\mu$m. The traces show the difference between using Prismspect and ABAKO to model the collisional radiative atomic kinetics. The main Kr Li-like transitions are labeled from A to D and are specified in Table I. The spectra are normalized to the most intense peak of line A.
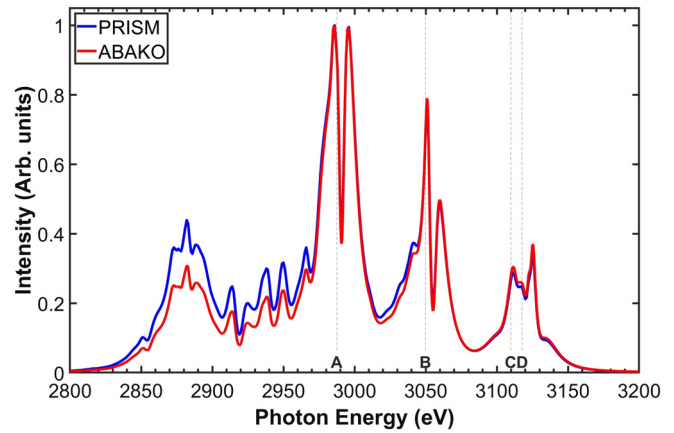
distribution normalized to the most intense peak of the Li-like transition A. The three lines represent three different plasma condition pairs of T_e and n_e for a uniform sphere. In this plot, we observe how the emergent intensity distribution changes when we keep one parameter fixed and change the other. Keeping T_e at 2 keV and increasing n_e from 5×10^{23} to 1×10^{24}/cc, we observe how the spectral lines change and increase their FWHM, while the relative emission between different ions is kept the same. This is the effect of the Stark broadening increase with the electron density. Keeping n_e at 1×10^{24}/cc and increasing T_e from 2 to 3 keV, we observe how the relative emission of Be-like lines decreases with respect to the Li-like ones, while the FWHM is practically unchanged. This is due to the shift in the charge state distribution toward higher charged states with increasing electron temperature.

Figure 16 shows the comparison between the emergent intensity distributions using Prismspect and ABAKO to model the collisional radiative atomic kinetics of the plasma. Both traces are for plasma conditions of $T_e = 2$ keV and $n_e = 10^{24}$/cc. We observe that ABAKO calculates a higher ionization in the plasma compared to Prismspect as there is more Li-like emission relative to the Be-like one. This discrepancy is consistent with Fig. 4 for the case of $T_e = 2$ keV. Considering that the selection of the atomic kinetic model influences the level populations, we have quantified the uncertainty arising from the differences between PrismSpect and ABAKO. This assessment was based on the comparison of the Be/Li-like population ratio curves depicted in Fig. 4. The model differences introduce an uncertainty of 5%–10% in T_e for the range of application. This difference in T_e does not significantly impact the Stark Broadening effect that determines the electron density.

V. CONCLUSIONS

This paper shows a series of results which provide a better understanding of the atomic physics and x-ray emission of Kr L-shell. Two different collisional-radiative models show an electron temperature sensitivity in the Be- and Li-like relative population which is reflected

in the relative intensity of the n = 4 to n = 2 line transitions. This sensitivity in the spectra is most appreciable in the range $T_e = [1.5 - 3]$ keV. The detailed Stark broadening calculations provide a more accurate modeling of the line-shapes of each transition and how they change with electron density. Results show sensitivity in the range $n_e = [5 \times 10^{23} - 2 \times 10^{24}]$/cc but might not be limited to it. The sensitivity of the Kr L-shell spectra to the plasma conditions can be used as a plasma spectroscopic diagnostic. More specifically, simulation results show it can be useful in implosion core experiments such as ICF in tracer concentrations between 0.02% and 0.04% in the plasma. These concentrations provide enough signal to be detected by x-ray spectrometers with spectroscopic quality while keeping opacity and hydrodynamic effects low. The combination of collisional-radiative and Stark broadening models provides an emergent intensity distribution which show both the T_e and n_e sensitivity. This distribution can be compared to the experimental spectra after applying the instrument response to infer the plasma conditions. The Stark broadened line shape presented here has emphasized the effect of static ions. The inclusion of ion dynamics is work in progress and will be reported elsewhere. They will impact the line profiles by filling valleys, rounding peaks, and adding a small increase in overall broadening.[37] However, they will not change the characteristic signatures of the static ions reported in this work.

The use of Kr L-shell as a spectroscopy diagnostic might prove useful in implosion cores where Ar K-shell becomes too ionized to be used ($T_e > 2$ keV). In addition, it may be used as a complementary diagnostic to Kr K-shell emission for T_e ranges for which they both are useful. The simultaneous detection of Kr K-shell and L-shell emission would provide a better understanding of the plasma charge state distribution and a more accurate plasma diagnostic due to the higher number of constraints when analyzing two different spectra. We would like to note that this spectral region overlaps with that of Si K-shell which may difficult the analysis in glass shell implosion capsules containing Si. Moreover, we would like to emphasize that in ablative thick shell experiments, where the core is confined by unablated, compressed shell material, the transmission of the Kr L-shell spectrum through it should be included in order to assess the impact on line intensity distribution.[6,7]

ACKNOWLEDGMENTS

AUTHOR DECLARATIONS
Conflict of Interest

The authors have no conflicts to disclose.

Author Contributions

E. Gallardo-Diaz: Formal analysis (lead); Investigation (lead); Writing – original draft (lead). **R. C. Mancini:** Formal analysis (supporting); Funding acquisition (equal); Investigation (supporting); Supervision (lead). **K. R. Carpenter:** Supervision (supporting). **P. Adrian:** Investigation (equal). **J. Frenje:** Funding acquisition (equal); Investigation (equal). **R. Florido:** Resources (equal); Supervision (supporting).

DATA AVAILABILITY

The data that support the findings of this study are available from the corresponding author upon reasonable request.

REFERENCES

[1]J. A. Frenje, R. Florido, R. Mancini, T. Nagayama, P. E. Grabowski, H. Rinderknecht, H. Sio, A. Zylstra, M. Gatu Johnson, C. K. Li, F. H. Séguin, R. D. Petrasso, V. Y. Glebov, and S. P. Regan, "Experimental validation of low-z ion-stopping formalisms around the bragg peak in high-energy-density plasmas," Phys. Rev. Lett. **122**, 015002 (2019).

[2]P. J. Adrian, R. Florido, P. E. Grabowski, R. Mancini, B. Bachmann, L. X. Benedict, M. G. Johnson, N. Kabadi, B. Lahmann, C. K. Li, R. D. Petrasso, H. G. Rinderknecht, S. P. Regan, F. H. Séguin, R. L. Singleton, H. Sio, G. D. Sutcliffe, H. D. Whitley, and J. A. Frenje, "Measurements of ion-electron energy-transfer cross section in high-energy-density plasmas," Phys. Rev. E **106**, L053201 (2022).

[3]R. Florido, T. Nagayama, R. C. Mancini, R. Tommasini, J. A. Delettrez, S. P. Regan, V. A. Smalyuk, R. Rodríguez, and J. M. Gil, "Analysis of time-resolved argon line spectra from omega direct-drive implosions," Rev. Sci. Instrum. **79**, 10E310 (2008).

[4]R. Florido, R. C. Mancini, T. Nagayama, R. Tommasini, J. A. Delettrez, S. P. Regan, and B. Yaakobi, "Spectroscopic modeling of an argon-doped shock-ignition implosion," Rev. Sci. Instrum. **81**, 10E307 (2010).

[5]R. Florido, R. Mancini, T. Nagayama, R. Tommasini, J. Delettrez, S. Regan, V. Smalyuk, R. Rodríguez, and J. Gil, "Argon k-shell and bound-free emission from omega direct-drive implosion cores," High Energy Density Phys. **6**, 70–75 (2010).

[6]R. Florido, R. C. Mancini, T. Nagayama, R. Tommasini, J. A. Delettrez, S. P. Regan, and B. Yaakobi, "Measurements of core and compressed-shell temperature and density conditions in thick-wall target implosions at the omega laser facility," Phys. Rev. E **83**, 066408 (2011).

[7]R. Florido, R. C. Mancini, T. Nagayama, R. Tommasini, J. A. Delettrez, and S. P. Regan, "Time-resolved characterization and energy balance analysis of implosion core in shock-ignition experiments at omega," Phys. Plasmas **21**, 102709 (2014).

[8]R. Florido and R. C. Mancini, "Assessment of transient effects on the x-ray spectroscopy of implosion cores at OMEGA," J. Phys. B: At., Mol. Opt. Phys. **48**, 224006 (2015).

[9]S. P. Regan, J. A. Delettrez, R. Epstein, P. A. Jaanimagi, B. Yaakobi, V. A. Smalyuk, F. J. Marshall, D. D. Meyerhofer, W. Seka, D. A. Haynes, I. E. Golovkin, and C. F. Hooper, "Characterization of direct-drive-implosion core conditions on OMEGA with time-resolved Ar k-shell spectroscopy," Phys. Plasmas **9**, 1357–1365 (2002).

[10]I. Golovkin, R. Mancini, S. Louis, Y. Ochi, K. Fujita, H. Nishimura, H. Shirga, N. Miyanaga, H. Azechi, R. Butzbach, I. Uschmann, E. Förster, J. Delettrez, J. Koch, R. W. Lee, and L. Klein, "Spectroscopic determination of dynamic plasma gradients in implosion cores," Phys. Rev. Lett. **88**, 045002 (2002).

[11]T. Ma, H. Chen, P. K. Patel, M. B. Schneider, M. A. Barrios, D. T. Casey, H.-K. Chung, B. A. Hammel, L. F. Berzak Hopkins, L. C. Jarrott, S. F. Khan, B. Lahmann, R. Nora, M. J. Rosenberg, A. Pak, S. P. Regan, H. A. Scott, H. Sio, B. K. Spears, and C. R. Weber, "Development of a krypton-doped gas symmetry capsule platform for x-ray spectroscopy of implosion cores on the NIF," Rev. Sci. Instrum. **87**, 11E327 (2016).

[12]H. Chen, T. Ma, R. Nora, M. A. Barrios, H. A. Scott, M. B. Schneider, L. Berzak Hopkins, D. T. Casey, B. A. Hammel, L. C. Jarrott, O. L. Landen, P. K. Patel, M. J. Rosenberg, and B. K. Spears, "On krypton-doped capsule implosion experiments at the national ignition facility," Phys. Plasmas **24**, 072715 (2017).

[13]M. J. May, G. E. Kemp, J. D. Colvin, D. A. Liedahl, P. L. Poole, D. B. Thorn, K. Widmann, R. Benjamin, M. A. Barrios, and B. E. Blue, "Investigation of high

x-ray conversion efficiency Kr filled gas sources at the national ignition facility," Phys. Plasmas **26**, 063105 (2019).

[14] L. Gao, B. F. Kraus, K. W. Hill, M. B. Schneider, A. Christopherson, B. Bachmann, M. Bitter, P. Efthimion, N. Pablant, R. Betti, C. Thomas, D. Thorn, A. G. MacPhee, S. Khan, R. Kauffman, D. Liedahl, H. Chen, D. Bradley, J. Kilkenny, B. Lahmann, E. Stambulchik, and Y. Maron, "Hot spot evolution measured by high-resolution x-ray spectroscopy at the national ignition facility," Phys. Rev. Lett. **128**, 185002 (2022).

[15] J. T. Clapp, R. C. Mancini, E. C. Harding, M. A. Schaeuble, and A. J. Harvey-Thompson, "Observation and diagnostic application of Kr K-shell emission in magnetized liner inertial fusion experiments at Z," Rev. Sci. Instrum. **93**, 103532 (2022).

[16] K. R. Carpenter, R. C. Mancini, E. C. Harding, A. J. Harvey-Thompson, M. Geissel, M. R. Weis, S. B. Hansen, K. J. Peterson, and G. A. Rochau, "Magnetic field impact on the laser heating in MagLIF," Phys. Plasmas **27**, 052704 (2020).

[17] K. R. Carpenter, R. C. Mancini, E. C. Harding, A. J. Harvey-Thompson, M. Geissel, M. R. Weis, S. B. Hansen, K. J. Peterson, and G. A. Rochau, "Temperature distributions and gradients in laser-heated plasmas relevant to magnetized liner inertial fusion," Phys. Rev. E **102**, 023209 (2020).

[18] H. M. Johns, R. C. Mancini, P. Hakel, T. Nagayama, V. A. Smalyuk, S. P. Regan, and J. Delettrez, Phys. Plasmas **21**, 082711 (2014).

[19] H. M. Johns, R. C. Mancini, T. Nagayama, D. C. Mayes, R. Tommasini, V. A. Smalyuk, S. P. Regan, and J. A. Delettrez, Phys. Plasmas **23**, 012709 (2016).

[20] S. Hansen, E. Harding, P. Knapp, M. Gomez, T. Nagayama, and J. Bailey, "Changes in the electronic structure of highly compressed iron revealed by x-ray fluorescence lines and absorption edges," High Energy Density Phys. **24**, 39–43 (2017).

[21] C. Keane, B. Hammel, A. Osterheld, R. Lee, D. Kania, L. Suter, R. Mancini, C. Hooper, and N. Delamater, "Analysis of K- and L-shell spectra from indirectly driven implosions," J. Quant. Spectrosc. Radiat. Transfer **51**, 147–159 (1994).

[22] C. Kaur, S. Chaurasia, N. Singh, J. Pasley, S. Aggarwal, and M. Mohan, "L-shell spectroscopy of neon and fluorine like copper ions from laser produced plasma," Phys. Plasmas **26**, 023301 (2019).

[23] E. V. Marley, D. A. Liedahl, M. B. Schneider, R. F. Heeter, L. C. Jarrott, C. W. Mauche, G. E. Kemp, M. E. Foord, Y. Frank, K. Widmann, and J. Emig, "Using L-shell x-ray spectra to determine conditions of non-local thermal dynamic equilibrium plasmas," Rev. Sci. Instrum. **89**, 10F106 (2018).

[24] E. E. Petkov, A. S. Safronova, V. L. Kantsyrev, V. V. Shlyaptseva, R. S. Rawat, K. S. Tan, P. Beiersdorfer, N. Hell, and G. V. Brown, "L-shell spectroscopic diagnostics of radiation from krypton HED plasma sources," Rev. Sci. Instrum. **87**, 11E315 (2016).

[25] S. B. Hansen, "Development and application of L-shell spectroscopic modeling for plasma diagnostics (order no. 3110887)," ProQuest Dissertations Theses Global 304619365 (2003). https://unr.idm.oclc.org/login?url=https://www.proquest.com/dissertations-theses/development-application-l-shell-spectroscopic/docview/304619365/se-2.

[26] J. MacFarlane, I. Golovkin, P. Woodruff, D. Welch, B. Oliver, T. Mehlhorn, and R. Campbell, "Simulation of the ionization dynamics of aluminum irradiated by intense short-pulse lasers," in *Proceedings of Inertial Fusion and Sciences Applications* (Sandia National Laboratory, 2003), Vol. 457.

[27] R. Florido, R. Rodríguez, J. M. Gil, J. G. Rubiano, P. Martel, E. Mínguez, and R. C. Mancini, "Modeling of population kinetics of plasmas that are not in local thermodynamic equilibrium, using a versatile collisional-radiative model based on analytical rates," Phys. Rev. E **80**, 056402 (2009).

[28] M. F. Gu, "The flexible atomic code," Can. J. Phys. **86**, 675–689 (2008).

[29] O. Peyrusse, J. Phys. B: At., Mol. Opt. Phys. **32**, 683 (1999).

[30] T. Nagayama, R. C. Mancini, R. Florido, R. Tommasini, J. A. Koch, J. A. Delettrez, S. P. Regan, and V. A. Smalyuk, "Processing of spectrally resolved x-ray images of inertial confinement fusion implosion cores recorded with multi-monochromatic x-ray imagers," J. Appl. Phys. **109**, 093303 (2011).

[31] T. Nagayama, R. Mancini, D. Mayes, R. Tommasini, and R. Florido, "An important criterion for reliable multi-monochromatic x-ray imager diagnostics and its impact on the reconstructed images," High Power Laser Sci. Eng. **3**, e23 (2015).

[32] R. Mancini, D. Kilcrease, L. Woltz, and C. Hooper, "Calculational aspects of the stark line broadening of multielectron ions in plasmas," Comput. Phys. Commun. **63**, 314–322 (1991).

[33] A. Kramida, "Cowan code: 50 years of growing impact on atomic physics," Atoms **7**, 64 (2019).

[34] B. Henry and H. Hora, "Polarization shift of spectral lines in high density plasmas," Opt. Commun. **44**, 185–187 (1983).

[35] C. A. Iglesias, H. E. DeWitt, J. L. Lebowitz, D. MacGowan, and W. B. Hubbard, "Low-frequency electric microfield distributions in plasmas," Phys. Rev. A **31**, 1698–1702 (1985).

[36] C. Iglesias, F. Rogers, R. Shepherd, A. Bar-Shalom, M. Murillo, D. Kilcrease, A. Calisti, and R. Lee, "Fast electric microfield distribution calculations in extreme matter conditions," J. Quant. Spectrosc. Radiat. Transfer **65**, 303–315 (2000).

[37] D. A. Haynes, D. T. Garber, C. F. Hooper, R. C. Mancini, Y. T. Lee, D. K. Bradley, J. Delettrez, R. Epstein, and P. A. Jaanimagi, "Effects of ion dynamics and opacity on stark-broadened argon line profiles," Phys. Rev. E **53**, 1042–1050 (1996).

[38] T. Burris-Mog, R. Mancini, J. Bailey, G. Chandler, G. Rochau, G. Dunham, P. Lake, K. Peterson, S. Slutz, T. Mehlhorn, I. Golovkin, and J. MacFarlane, "Line broadening analysis of implosion core conditions at z using argon k-shell spectroscopy," J. Quant. Spectrosc. Radiat. Transfer **99**, 120–130 (2006).

18 March 2024 23:03:41